Energy transfer dynamics in trimers and aggregates of light-harvesting complex II probed by 2D electronic spectroscopy

Miriam M. Enriquez, Parveen Akhtar, Cheng Zhang, Győző Garab, Petar H. Lambrev, and Howe-Siang Tan

Citation: The Journal of Chemical Physics **142**, 212432 (2015); doi: 10.1063/1.4919239
View online: http://dx.doi.org/10.1063/1.4919239
View Table of Contents: http://scitation.aip.org/content/aip/journal/jcp/142/21?ver=pdfcov
Published by the AIP Publishing

Energy transfer dynamics in trimers and aggregates of light-harvesting complex II probed by 2D electronic spectroscopy

Miriam M. Enriquez,[1] Parveen Akhtar,[2] Cheng Zhang,[1] Győző Garab,[2] Petar H. Lambrev,[2,a)] and Howe-Siang Tan[1,b)]
[1]*Division of Chemistry and Biological Chemistry, School of Physical and Mathematical Sciences, Nanyang Technological University, Singapore 637371*
[2]*Institute of Plant Biology, Biological Research Centre, Hungarian Academy of Sciences, P.O. Box 521, H-6701 Szeged, Hungary*

(Received 6 February 2015; accepted 15 April 2015; published online 4 May 2015)

The pathways and dynamics of excitation energy transfer between the chlorophyll (Chl) domains in solubilized trimeric and aggregated light-harvesting complex II (LHCII) are examined using two-dimensional electronic spectroscopy (2DES). The LHCII trimers and aggregates exhibit the unquenched and quenched excitonic states of Chl *a*, respectively. 2DES allows direct correlation of excitation and emission energies of coupled states over population time delays, hence enabling mapping of the energy flow between Chls. By the excitation of the entire Chl *b* Q_y band, energy transfer from Chl *b* to Chl *a* states is monitored in the LHCII trimers and aggregates. Global analysis of the two-dimensional (2D) spectra reveals that energy transfer from Chl *b* to Chl *a* occurs on fast and slow time scales of 240–270 fs and 2.8 ps for both forms of LHCII. 2D decay-associated spectra resulting from the global analysis identify the correlation between Chl states involved in the energy transfer and decay at a given lifetime. The contribution of singlet–singlet annihilation on the kinetics of Chl energy transfer and decay is also modelled and discussed. The results show a marked change in the energy transfer kinetics in the time range of a few picoseconds. Owing to slow energy equilibration processes, long-lived intermediate Chl *a* states are present in solubilized trimers, while in aggregates, the population decay of these excited states is significantly accelerated, suggesting that, overall, the energy transfer within the LHCII complexes is faster in the aggregated state. © *2015 AIP Publishing LLC.* [http://dx.doi.org/10.1063/1.4919239]

I. INTRODUCTION

The process of photosynthesis is initiated by the absorption of light and efficient transport of energy by pigment–protein antenna complexes embedded in the thylakoid membranes.[1] In green plants, the major and most abundant antennas are the trimeric light-harvesting complex II, LHCII, located on the periphery of the reaction center of Photosystem II (PSII). Identifying the precise dipole moment orientations and distances of pigments based on the molecular structure of LHCII has been an important key to assigning the interacting pigments in the stromal and lumenal layers for efficient light harvesting and energy transfer functions.[2,3] In addition, modelling the excitonic couplings and site energies of the 14 chlorophylls (Chls) based on the crystal structure[2,4] has been used to predict the downhill Chl energy transfer routes and ultrafast dynamics.[5–9]

In addition to the light-harvesting function, LHCII is involved in the non-radiative dissipation of excess excitation energy, a process collectively referred to as non-photochemical quenching (NPQ) of Chl fluorescence,[10–12] a key mechanism for protection against photodamage under excess radiation levels. *In vitro*, significant quenching manifested in shortening of the Chl *a* excitation lifetime[13–16] and development of a far-red emitting state[17,18] are observed upon protein aggregation of LHCII. Aggregation of LHCII in solution by means of removal of detergent provides a good *in vitro* model of LHCII in the quenched state. The molecular mechanism behind NPQ has so far not been unequivocally established[19] and there may, in fact, be several mechanisms acting in parallel, such as decay via the S_1 state of lutein[3,20] and via a Chl–Chl charge transfer state;[17,18,21] other mechanisms have been proposed as well.[22–24]

While a great amount of effort has been centered on explaining the precise mechanism of quenching the excess excitation energy of Chls, in-depth analyses on examining the Chl energy transfer process in the quenched state of LHCII are scarce. Femtosecond transient absorption spectroscopy studies on LHCII aggregates previously using Chl *a* excitation have led to proposals of models and dynamics of energy flow to the intermediate quencher state, be it either a carotenoid S_1 state[20] or a Chl–Chl charge transfer state.[21] Recent transient absorption measurements on LHCII also showed no significant changes on the spectra and dynamics of excitation energy transfer from carotenoid upon protein aggregation of LHCII complexes.[16] On the other hand, the presence of Chl–Chl and possibly Chl–Car charge-transfer states has been recently confirmed by Stark spectroscopy[25] and spectral hole-burning.[26] Regardless of the mechanism of dissipation, there is ample evidence that structural changes within the LHCII

a)Electronic mail: lambrev@brc.hu
b)Electronic mail: howesiang@ntu.edu.sg

protein complex activate the quenching, although an agreement does not seem to exist in the literature on this question either. No studies on the energy transfer dynamics and excitonic coupling between Chls *a* and *b* in LHCII aggregates have been reported so far. In this present work, we aimed to verify whether and how aggregation alters the pathways and energy transfer dynamics within the complexes when compared to the unquenched, detergent-solubilized state.

Chl energy transfer pathways and dynamics in the unquenched trimeric LHCII have been extensively studied using pump–probe spectroscopy.[5,27–29] Similar dynamics of energy transfer were obtained in monomeric LHCII, indicating energy transfer processes within the monomeric subunits.[30] While pump–probe technique has been proven useful for studying Chl excited states, in the case of spatially unresolved Chl excitonic states, pump–probe spectroscopy alone cannot directly provide information on which Chl excitonic states are coupled.

Fourier transform two-dimensional electronic spectroscopy (2DES)[31–34] provides a more detailed picture of the precise correlations of coupled Chl excitonic states by studying evolution in the cross peak signal at different time delays. The two frequency axes in a 2D spectrum enable direct correlation of the excitation and emission energies of coupled states, thus revealing excited state population transfer from one state to another. Multiple energy transfer routes and couplings in LHCII have been analyzed using 2DES at low temperature.[35,36] More recently, 2DES has been used to study the kinetics and pathways of energy transfer from Chl *b* to Chl *a* in LHCII trimers at physiological temperature, by selectively exciting the entire Chl *b* band.[37] As a follow-up to this study, we applied the same excitation to both LHCII trimers and aggregates and monitored the excitation energy transfer from Chl *b* to Chl *a* by the same 2DES technique. We examine how the change in the environment and possibly conformation of the LHCII complex upon aggregation affects the energy transfer routes and excitonic couplings on the ultrafast time scales. While the general characteristics of Chl energy transfer remain in the aggregated state, specific changes in the dynamic population of intermediate-energy Chl *a* states could be identified.

II. MATERIALS AND METHODS

A. Sample preparation

LHCII trimers were isolated and purified by sucrose density gradient ultracentrifugation using PSII-enriched membrane fragments (so called BBY particles) isolated from pea (*Pisum sativum*) as starting material according to Caffari *et al.*[38] Suspensions of BBY at about 0.5 mg/ml Chl were solubilized with 0.6% α-dodecyl maltoside (α-DM), and the sample was loaded on sucrose gradient. The gradient was prepared by repetitive freezing and thawing of a mixture containing 0.4 M sucrose, 10 mM tricine buffer, 0.06% α-DM, and pH 7.8. The samples were centrifuged in a swing-out rotor at 200 000 g for 20 h. Fractions of the gradient containing the LHCII trimer bands were collected, concentrated with 30 kDa cutoff Amicon filters (Millipore), and stored at −80 °C until use. Aggregates were prepared by removing the detergent from the solubilized LHCII solution with the absorbing beads (Bio-Beads SM-2, Bio-Rad). LHCII suspension at 30–50 μg/ml Chl in 20 mM tricine buffer was incubated at room temperature with 80–90 mg/ml Bio-Beads for at least 2 h with continuous stirring.

Sample solutions of LHCII trimers and aggregates were adjusted to an optical density equivalent to 0.2 at the Chl *b* Q_y band (650 nm) in a 1 mm path length. Photo-oxidation of the sample during the measurements was minimized by using oxygen-scavenging system consisting of 165 U/ml glucose oxidase, 2170 U/ml catalase, and 0.5% glucose.

B. Time-resolved fluorescence

Fluorescence decays were recorded at room temperature with an effective time resolution of 5-10 ps by time-correlated single-photon counting (TCSPC) using a FluoTime 200 instrument (PicoQuant, Germany). Excitation pulses of 6 ps duration, 20 MHz repetition rate, and 633 nm wavelength were given by a WhiteLase micro supercontinuum laser (Fianium, UK). Fluorescence emission was detected through a monochromator at 680 nm. Lifetime analysis was done in MATLAB using homemade routines.

C. 2D electronic spectroscopy

2DES was carried out using a femtosecond laser system in a partially collinear pump–probe beam geometry setup as previously described.[39–41] Briefly, a Ti:sapphire regenerative amplifier (Legend Elite, Coherent), seeded by modelocked pulses from a Ti:sapphire oscillator (Micra, Coherent), produces pulses centered at 800 nm at 1 kHz repetition rate. The output laser pulse, having 0.8 mJ pulse energy and 40 fs pulse duration, is used to pump a two-stage, home-built optical parametric amplifier (OPA). Near infrared signal generated from the OPA is frequency doubled to obtain 650 nm pump pulse with ~15 nm bandwidth to provide excitation to the entire Chl *b* Q_y region. The pump excitation spectrum overlaid with the linear absorption spectra of LHCII trimers and aggregates in the Chl Q_y region is illustrated in Fig. 1.

The excitation beam is directed to an acousto-optic programmable dispersive filter (AOPDF) pulse shaper[42,43] (Dazzler, Fastlite) to generate the first two collinear interaction pulses at varied coherence time delays t_1 and relative phases. Compression by the pulse shaper yielded pump pulses with 55 fs pulse duration. The first two excitation pulses were attenuated to 15 nJ energy per pulse and scanned from 0 to 150 fs t_1 delay with increments of 3 fs steps. Data collection over t_1 was taken using a partially rotating frame with reference wavelength set at 730 nm. Background-free 2D signals were acquired using a 1×2 phase-cycling scheme as previously discussed.[39,40] To investigate for the presence and effect of singlet–singlet annihilation process in the measurements, 2D spectra of the samples were also recorded using laser excitation energies of 10 and 65 nJ per pulse.

The probe pulse is generated from a white light continuum produced by focusing a small fraction of the amplified 800 nm beam on a 2 mm sapphire window. The excitation dynamics is recorded by controlling the time delay of the probe pulse

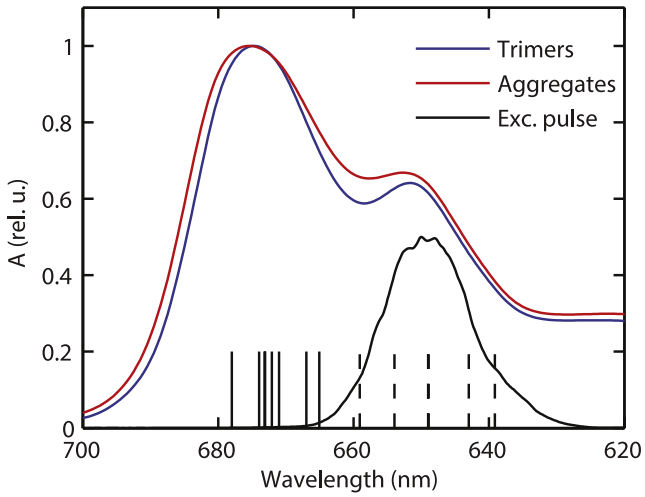

FIG. 1. Normalized linear absorption spectra in the Chl Q_y region of LHCII trimers in aqueous buffer solution containing 0.03% dodecyl maltoside and of aggregates in detergent-free buffer, overlaid with the spectrum of the excitation pulses used for 2DES measurements. The energy level positions of Chl *a* (solid lines) and Chl *b* (dashed lines) exciton states in trimeric LHCII are included in the plot.[7]

with respect to the second excitation pulse, referred as waiting time t_2, with a motorized delay stage. The probe beam is spatially overlapped with the pump beam on the sample and sent to a spectrometer (Acton SP2300, Princeton Instruments) equipped with a CCD detector (Pixis 100B, Princeton Instruments) to spectrally resolve the signal. LHCII samples were recycled through a flow cell of 1 mm optical path length to ensure that the pump beam excites different portions of the sample during data collection. 2D spectra were recorded up to $t_2 = 800$ ps. Linear absorption spectra were taken before and after measurements to check for the sample integrity. Correction for dispersion of the probe light and global fitting analysis of the 2D spectra were carried out in MATLAB using a method described in Ref. 37.

III. RESULTS

A. Purely absorptive 2D spectra

2DES provides direct correlations of electronic couplings between pigments within the excitation coherence during time t_1 and the emission coherence during time t_3. Fourier transformation along t_1 produces the pump excitation frequency axis. Here, the electronic signals from the measurements are plotted in terms of excitation wavelength λ_1 on the vertical axis and detection wavelength λ_3 on the horizontal axis. The purely absorptive 2D spectra of LHCII trimers and aggregates recorded at waiting times t_2 of 300 fs, 3 ps, and 30 ps are presented in Fig. 2. The 2D spectra are plotted using identical contour and color intensity scale for convenience of comparison. In the 2D spectra, the peaks along the white dashed line (diagonal peaks) correspond to the linear absorption position of Chl *b* Q_y band, which is within the spectral range of the excitation pulse, whereas the peaks in the off-diagonal region (cross peaks) result from couplings and energy transfer between Chl excitonic states. Since our first two excitation pulses did not cover the spectral range of the Chl *a* Q_y band (Fig. 1), neither diagonal peaks nor quantum coherences[44,45] due to Chl *a* were observed in the 2D spectra; hence, the range of λ_1 wavelengths above 665 nm is not included in the plots. Although certain overlap exists between the vibronic Q_y band of Chl *a* and the main Q_y absorption band of Chl *b*, the intensity of the vibronic band is much lower; hence, direct excitation of Chl *a* states is negligible.

Photosynthetic light-harvesting systems usually follow a downhill excitation population transfer probed along $t_2 > 0$. The cross peaks in the 2D spectra provide information on the connectivity of excitons from initially excited Chl *b* to Chl *a* states. Due to large spectral overlap of exciton transition bands in the spectrum, we cannot unambiguously assign the peaks corresponding to a single exciton state. However, the cross peak signals provide substantial information on which Chl spectral regions are energetically coupled.

The decrease of the diagonal peak signal along the white dashed line during time evolution is accompanied by an increase of the cross peak signal corresponding to Chl *a* bleaching, peaking at around $\lambda_3 = 680$ nm. The rise of Chl *a* bleaching is indicative of energy transfer taking place between the coupled Chl pigments. At ultrafast timescale of 300 fs in Fig. 2, the cross peaks in both LHCII trimers and aggregates are noticeably asymmetrical with respect to the excitation wavelength λ_1. The asymmetry is due to the higher intensity found at the intersection $\lambda_1 = 655$ nm and $\lambda_3 = 665$ nm. The negative signal at intersections $\lambda_1 \rightarrow \lambda_3$ generally indicates energy flow from initially excited Chl *b* states at wavelength λ_1 to acceptor Chl *a* states at λ_3. The signal intensity is more pronounced at the cross peak intersection 655 → 665 nm, than at 645 → 665 nm, suggesting that for both trimers and aggregates, the deactivation of Chl *b* excited states proceeds through different pathways. Excitation energy originating from Chl *b* states at $\lambda_1 = 645$ nm directly populates low-lying Chl *a* states around $\lambda_3 = 680$ nm, whereas energy from Chl *b* states at $\lambda_1 = 655$ nm flows through intermediate energy states at $\lambda_3 \geq 660$ nm.

For both LHCII preparations, the Chl *b* diagonal peaks are nearly undetectable in the 2D spectra at delay time of 3 ps, while the intensity of the main Chl *a* cross peak is increased, indicating that excitation energy from Chl *b* has been transferred to Chl *a* over this time period. However, there is still pronounced intensity at the 655 → 660 nm intersection, showing that energy transfer from the 660 nm state to lower energy Chls is markedly slower. Significant differences between the detergent-solubilized trimers and aggregated LHCII were not observed in these 2D spectra. At 30 ps waiting time, the cross peak shape is almost symmetric revealing the (quasi) equilibrium population of Chl *a* states. The signal intensity in LHCII aggregates is obviously lower owing to the faster decay to the ground state in those quenched samples.

B. Global analysis

In order to gain insight into the temporal evolution of the 2D spectra and hence on the kinetics of energy transfer and relaxation process of Chl excitonic states in LHCII, global lifetime analysis of the time series of 2D absorptive spectra[37] was performed in LHCII trimers and aggregates. The global

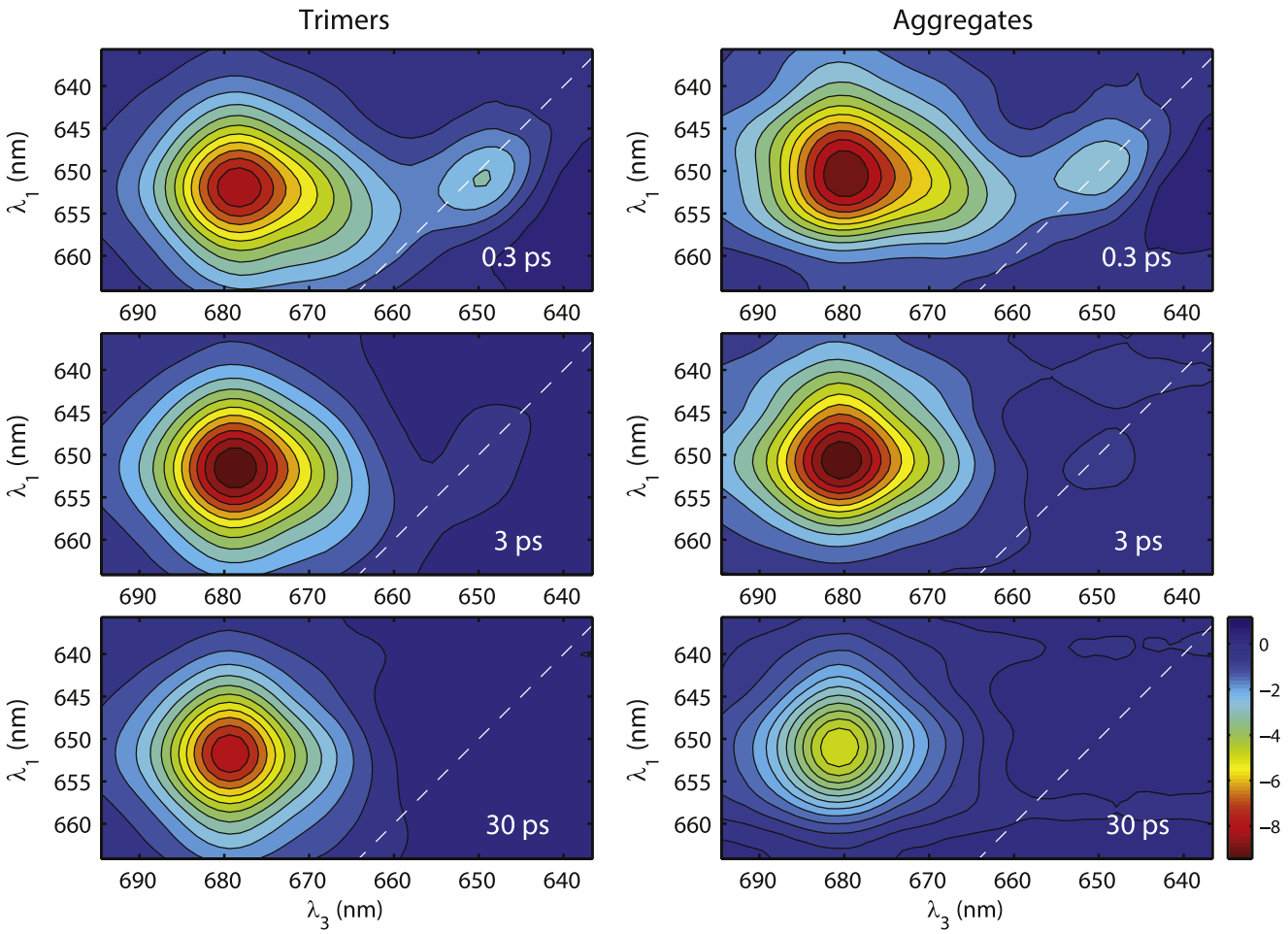

FIG. 2. Purely absorptive 2D spectra of LHCII trimers (left column) and aggregates (right column) recorded in the Chl Q_y region at 300 fs, 3 ps, and 30 ps waiting times (t_2). The 2D spectra are plotted in terms of excitation wavelength λ_1 and detection wavelength λ_3.

fitting was carried out for 2D spectra recorded from 150 fs to 800 ps. For both samples, four kinetic decay components were required to obtain satisfactory fits to the 2D spectra. An additional component, compared to previous analyses,[37] was necessary due to the broader delay time range used here. The results of the global analysis provide characteristic lifetimes of the system kinetics, and the 2D decay-associated spectra (2D DAS) describe the correlation between the Chl excitonic states actively participating in the kinetics at a given lifetime. 2D DAS and the respective lifetimes are compared for LHCII trimers and aggregates in Fig. 3. The 2D DAS reveal characteristic spectral profiles of intermediate states that are not readily identified just by inspecting the 2D spectra alone. The absorptive 2D signal is dominated by the negative ground-state bleaching and consequently the amplitudes of 2D DAS show dynamic changes of the bleaching signal. Negative amplitude of 2D DAS, represented by red color, thus indicates decay of the bleaching signal, whereas positive amplitude of 2D DAS, coded in blue color, indicates that the amplitude of the bleaching grows with the given lifetime.

The first 2D DAS of trimers (Fig. 3(a)) and aggregates (Fig. 3(e)), corresponding to lifetimes of 270 and 240 fs, respectively, are very similar. Excitation energy transfer between strongly coupled Chl *b* and Chl *a* excitonic states is evident on this time scale. The negative (λ_3 = 640–665 nm) and positive (λ_3 = 670–690 nm) signals correspond to the decay of Chl *b* and rise of Chl *a* bleaching signal, respectively. The second 2D DAS (Figs. 3(b) and 3(f)) reflect slower energy transfer pathways between Chls, occurring on a time scale of ~2.8 ps. In contrast to the first 2D DAS (Figs. 3(a) and 3(e)), the slow energy transfer from Chl *b* to Chl *a* is mediated by intermediate energy Chls which are evident by the appearance of negative cross peak intensity around λ_3 = 660–675 nm. In solubilized trimers, the intermediate intensity is found between λ_3 = 660 and 667 nm (15 150–15 000 cm^{-1}) and strongly coupled to lower-energy Chl *b* absorbing at λ_1 = 654–656 nm (~15 300 cm^{-1}). In aggregates, however, additional negative amplitude can be observed in the range λ_3 = 665–675 nm (~15 000–14 800 cm^{-1}), testifying that lower-energy Chl *a* exciton states relax on this time scale in aggregates. Comparing the amplitude of the negative diagonal peak signal of Chl *b* in the first and second 2D DAS, majority of the excitation energy from Chl *b* is transferred to Chl *a* at the more rapid time scale of 240–270 fs. Figure 4 will provide more details of the results of the second 2D DAS.

The third 2D DAS of trimers (Fig. 3(c)) and aggregates (Fig. 3(g)) decay around 14–15 ps and are characterized by a broad negative cross peak at the detection wavelength of 665–690 nm, signifying decay of the Chl *a* Q_y bleaching signal. The cross peak in trimers (Fig. 3(c)) is noticeably broader

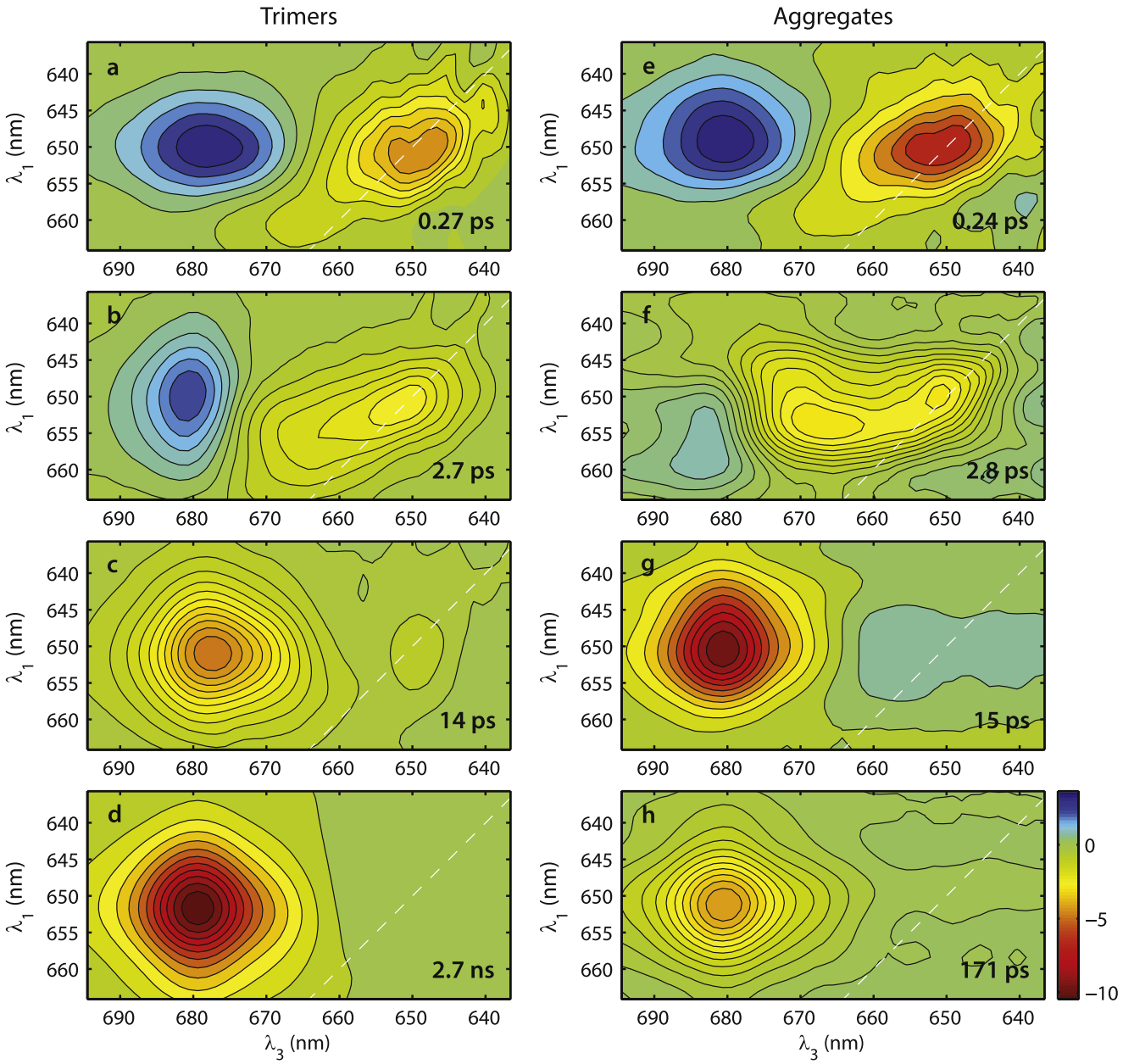

FIG. 3. 2D DAS of LHCII trimers (a)–(d) and aggregates (e)–(h) resulting from global lifetime analysis of a series of 2D spectra at t_2 from 150 to 800 fs with four exponential decay components. The decay lifetimes are indicated on the plots.

on the short-wavelength side, in the region of 655 → 667 nm (15 300 → 15 000 cm^{-1}) intersection, indicating the presence of long-lived intermediate exciton states. In contrast, the aggregates 2D DAS (Fig. 3(g)) do not have sizeable amplitude in the region of 655 → 667 nm, since the population of the corresponding energy levels decays on a faster time scale, as evidenced by the 2.8 ps 2D DAS.

The 14–15 ps component of 2D DAS can be attributed to a combination of energy equilibration of a portion of excited state population from weakly connected Chls to the lowest Chl excited state, and singlet–singlet annihilation, occurring when two migrating excited states collide within their lifetime.[28,46,47] The third component of 2D DAS has significantly larger amplitude in aggregates. This is most likely because in aggregated LHCII, excited states can jump over adjacent complexes migrating over a much larger domain size,[47,48] thus increasing the likelihood for annihilation. For LHCII aggregates, the effective domain size is about 20× larger than the trimers, hence the much greater 15 ps contribution due to the singlet–singlet annihilation.

The final 2D DAS reflect the slow decay of the lowest energy Chl *a* exciton states to the ground state. Accordingly, in trimers, the decay lifetime was found around 3 ns (Fig. 3(d)), whereas in the quenched aggregates, it was reduced to ~170 ps (Fig. 3(h)). Thus, the final lifetimes are consistent with the bulk of experimental data on aggregated and trimeric LHCII.[13,14,16,17,20,21]

It is evident from the 2D DAS that, apart from the well-known shortening of the overall excited-state lifetime, LHCII aggregates are characterized by a change in excited-state dynamics of Chl *a* occurring on the picosecond time scale, evidenced by a change in the shape of the 2.8 ps 2D DAS. The

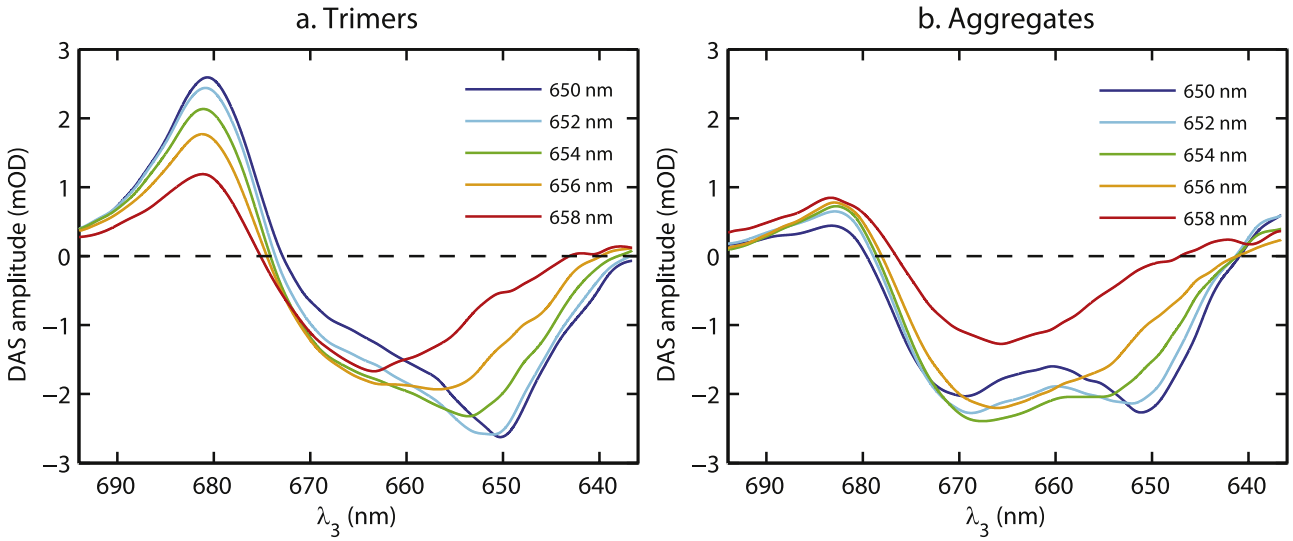

FIG. 4. Horizontal slices at selected excitation wavelengths λ_1 of the second component of 2D DAS (2.8 ps) of LHCII trimers (a) and aggregates (b) from Figs. 3(b) and 3(f), respectively.

spectral shape of the 2.8 ps 2D DAS is illustrated in Fig. 4 in the form of a set of slices at different λ_1 and compared with solubilized trimers. The intermediate negative peak for trimers is positioned near $\lambda_3 = 665$ nm and is only distinctly pronounced for $\lambda_1 > 654$ nm. In aggregates, on the other hand, the spectra show a strong negative peak at $\lambda_3 = 670$ nm which is correlated with $\lambda_1 = 650$–656 nm and a weaker positive amplitude at 680 nm, representing the rise of lower-energy Chl *a* state population.

C. 2D spectra obtained with high power excitation pulses

In order to evaluate the contribution of singlet–singlet annihilation to the kinetics of excited-state decay, 2D spectra of aggregates and trimers were also measured using lower and higher excitation pulse energies (10 nJ and 65 nJ). The probability for multiple excitations within the pulse duration grows with the pulse energy and so does the probability for annihilation. The same global analysis procedure with four kinetic components was applied to the 2D spectra. While lower energies yielded qualitatively similar 2D DAS (supplementary material[57]), there were notable differences at 65 nJ (Fig. 5). Differences in the spectral profiles are evident in the longer lifetime components, particularly the second 2D DAS (Figs. 5(b) and 5(f)). At high pulse energies, the 2D DAS for both trimers and aggregates reveal decay in a broad range of wavelengths between 660 and 680 nm, whereas the 2D DAS for low-power measurements (Figs. 3(b) and 3(f)) showed a clear rise in the Chl *a* excited-state population. Another apparent difference is that the relative amplitude of the 21–22 ps 2D DAS at high power (Figs. 5(c) and 5(g)) is significantly higher, compared to the relative amplitude of the 14–15 ps 2D DAS at low power (Figs. 3(c) and 3(g)). Even in solubilized trimers, the 15–20 ps lifetime component represents the predominant pathway for excitation energy decay at high pulse energies. It can be concluded that singlet–singlet annihilation is one reason for the observed excited state decay on the time scales of 2–3 ps and especially 15–20 ps in the high power excitation measurements.

IV. DISCUSSION

In the present work, we investigated the energy transfer pathways and dynamics in LHCII trimers and aggregates using 2DES. Rather than focusing on the lowest-lying energy states responsible for quenching, we directed our attention to the overall energy transfer dynamics starting from excited Chl *b*. Since Chl *b* molecules interact with neoxanthin on the lumenal side of LHCII and neoxanthin is known to undergo conformational changes upon aggregation,[49] it is reasonable to expect that energy transfer from Chl *b* will be also affected, especially since aggregates display marked changes in their circular dichroism spectra in the Chl *b* region.[50–52] However, our 2DES results did not reveal any gross changes in the time scale of energy transfer or Chl *b*–Chl *a* couplings in aggregated compared to solubilized LHCII, which both display similar spectral evolution on the time scale of 0.2–0.3 ps (compare the 2D DAS in Figs. 3(a) and 3(e)). Furthermore, the intermediate energy 2D cross-peak (Fig. 3(b)), reported earlier for trimers,[37] is also observed in aggregates (Fig. 3(f)), similarly found at $\lambda_3 = 660$–665 nm and coupled to low energy Chl *b* states at $\lambda_1 = 654$–656 nm.

A. Two long-lived intermediate energy states

In our experiments, an even longer-lived Chl *a* intermediate state was resolved, absorbing at around 670–675 nm, which equilibrates with the lowest-energy exciton states on the time scale of 15 ps (the value is probably not exact since this lifetime is primarily dominated by singlet–singlet annihilation). Exciton energy transfer models based on Redfield/modified Redfield theory predict generally faster equilibration times,[5] but slow energy transfer between Chl *a* states, on the time scale of tens of picoseconds, has been estimated by Renger *et al.*[8] applying generalized Förster theory. Based on

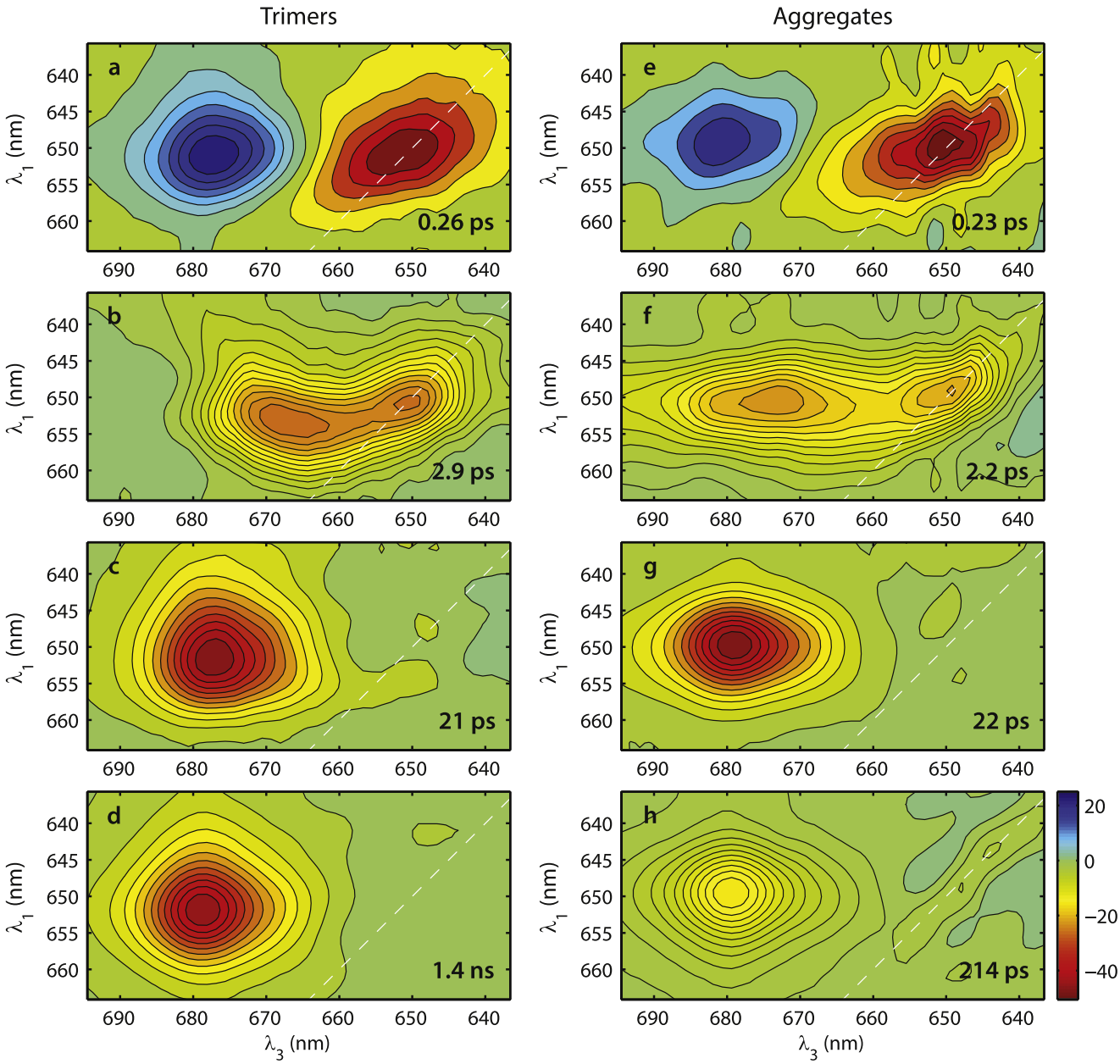

FIG. 5. 2D decay-associated spectra of LHCII trimers (a)–(d) and aggregates (e)–(h) resulting from global analysis of 2D spectra obtained using excitation pulses of 65 nJ energy.

the comparative global analysis of the 2D spectra of trimers and aggregates, we propose that the long-lived intermediate state at 670–675 nm decays faster in aggregates, on time scale of ~3 ps, as opposed to ~15 ps in trimers. This conclusion is mainly based on the pronounced negative amplitude in the 2.8 ps 2D DAS of aggregates at the intersection 650 → 670 nm (Figs. 3(f) and 4(b)) and, respectively, the lack of the respective cross-peak amplitude in the 15 ps 2D DAS (Fig. 3(g)). It must be noted that this intermediate state (670–675 nm) has a different identity than the intermediate state at 660–670 nm (Fig. 3(b), discussed also in earlier works on LHCII[35,37,53]). The long-lived state is not only distinguished by its longer lifetime (in trimers) and lower energy but also because it has stronger coupling to Chl *b* states absorbing at ~650 nm than at ~655 nm. The latter characteristic is the reason why this state is readily resolved by 2DES.

The 2D DAS show that the intermediate state population decays but do not necessarily reveal the fate of the excitation energy. There can be several reasons for the accelerated decay in aggregated LHCII. The excitations could decay by ultrafast internal conversion to the ground state, in which case, this intermediate state would be an effective quencher, or, more likely, by relaxation to another Chl *a* exciton state, carotenoid molecule, or a mixed (charge-transfer) state. Another possibility that needs to be considered is that the apparent decay is due to singlet–singlet annihilation in the aggregates.

B. Contribution of singlet-singlet annihilation to the excited-state decay

Previous time-resolved studies on LHCII aggregates[21,54] have demonstrated that annihilation is mostly relevant on a

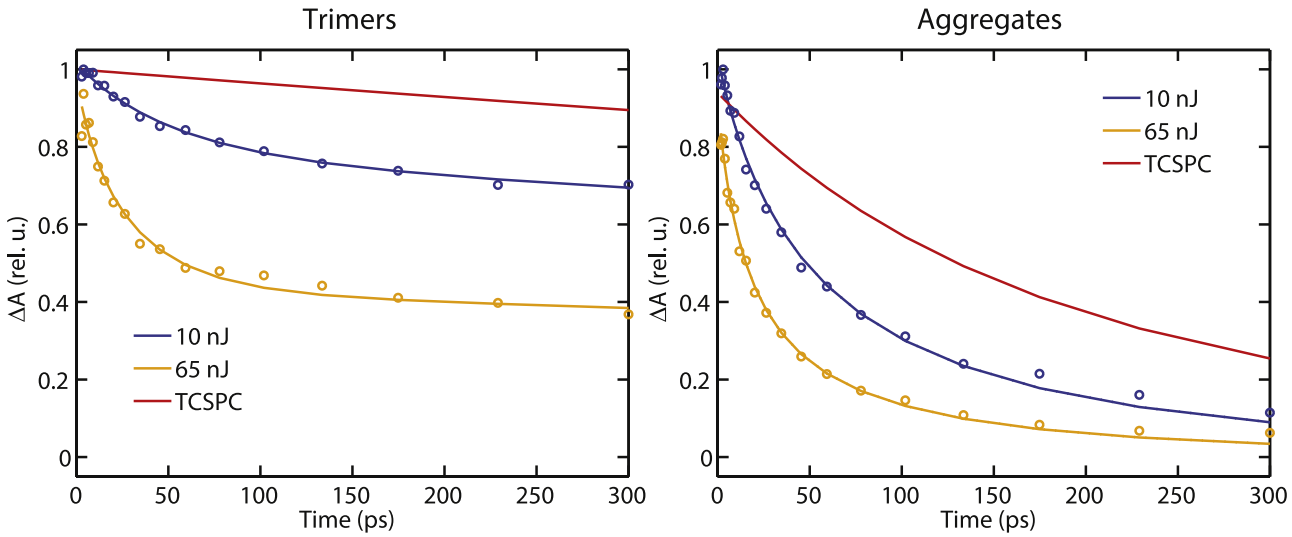

FIG. 6. Experimental kinetic traces (circles) of integrated 2D signals at the Chl *a* band of trimers and aggregates taken at low and high power excitations, overlaid with fits (lines) resulting from modelling of the annihilation kinetics. The estimated reciprocal annihilation rate constants (γ^{-1}) are 60 ps for the trimers and 38 ps for the aggregates. The red lines represent the simulated Chl *a* decay based on TCSPC measurement shown in Fig. S2.[57]

time scale of tens to hundreds of picoseconds but due to its non-exponential kinetics, it may influence the shorter-lived lifetime components as well.[21] The 2DES measurements performed at high excitation energy (65 nJ) clearly demonstrate that singlet–singlet annihilation has significant impact on the kinetics even on a time scale of 2–3 ps. Rather than rising, the population of low-energy Chl *a* states decays with a 2–3 ps lifetime in aggregates and, to a lesser extent, trimers. It is thus a viable hypothesis that the enhanced 3-ps decay found in aggregates at 15 nJ pulse energy is also simply due to inter-trimer exciton migration and annihilation. To evaluate this hypothesis, we compare the 2DES results obtained at lower energy excitation of 10 nJ (Figure S1[57]) from the same samples and with the same experimental conditions (other than pulse energy) as the 65 nJ results. The results obtained from 10 nJ energy excitation, having lifetimes and 2D DAS features very similar to those obtained at 15 nJ. We note, however, that the errors of fit for the 10 nJ data are relatively high (Table S1 in the supplementary material[57]), especially for the third and fourth decay components. The data are useful for quantitative comparison of the contribution of singlet–singlet annihilation to the kinetics. To this end, we applied the approach described in the work of Barzda *et al.*,[47] of fitting a kinetic model including annihilation to the transient absorption data and determining the second-order kinetic rate constant of annihilation for trimers and aggregates.

The inverse rate constants of singlet–singlet annihilation (γ^{-1}) of LHCII were previously found to be in the range of 24–86 ps in solubilized trimers and 16–18 ps in aggregates.[47,54,55] A description of our annihilation rate analysis can be found online in the supplementary material.[57] To evaluate the annihilation rate constants in our samples, we used the annihilation-free excited-state decay parameters (lifetimes and amplitudes) of the solubilized and aggregated LHCII samples measured by time-resolved fluorescence (TCSPC) using 0.1 pJ excitation pulses (Fig. S2[57]). These were used as fixed parameters in the annihilation model, which additionally included the nonlinear decay rate constant γ, initial excitation density (average number of excited trimers per pulse) n_0, and, for aggregates only, the structural dimension parameter d_s. These parameters were varied to obtain the best fit of the simulated kinetic curves with the time dependence of the integrated (along λ_1) 2D signal at the Chl *a* band (677–683 nm) measured at low (10 nJ) and high (65 nJ) excitation pulse energies. The so-called statistical model was applied to describe annihilation in trimers and a kinetic model was applied for aggregates.[47] The simulated decay traces overlaid on the experimental integrated transients are plotted in Fig. 6. The estimated inverse annihilation rate constants are γ^{-1} = 60 ps for solubilized trimers and γ^{-1} = 38 ps for aggregates. Consistent with previous studies,[47,55] the quenched form of LHCII seems to promote faster annihilation rate, which has been explained as being the result of conformational changes affecting the rate of inter-monomer energy equilibration. The fits also accurately model the observation that in trimers, annihilation only occurs within the early timescales (<100 ps), whereas in the aggregates, owing to their large domain size, annihilation can be observed over the entire timescale of Chl *a* excitation decay.

Given the annihilation rate constants of trimers and aggregates, we assess their respective contribution to the picosecond energy transfer dynamics by fitting exponential decay functions to the simulated annihilation kinetic curve (see supplementary material[57]). The fits to the annihilation decay curve in trimers (based on γ^{-1} = 60 ps) have no fast-decaying component around 3 ps, indicating that there is no contribution of annihilation on this sample. Due to the faster annihilation rate constant of aggregates (γ^{-1} = 38 ps), the corresponding annihilation decay curve exhibits a decay component of ~3 ps with a small relative amplitude (~5%). Hence, we can conclude that the contribution of annihilation to the 3 ps 2D DAS of aggregates is minimal.

Another way to test whether annihilation could account for the observed picosecond decay of the intermediate state is simply by inspecting the measured time traces at excitation wavelength of 672 nm and 680 nm and the simulated annihilation decay curve in a 0–5 ps region (Fig. 7). The

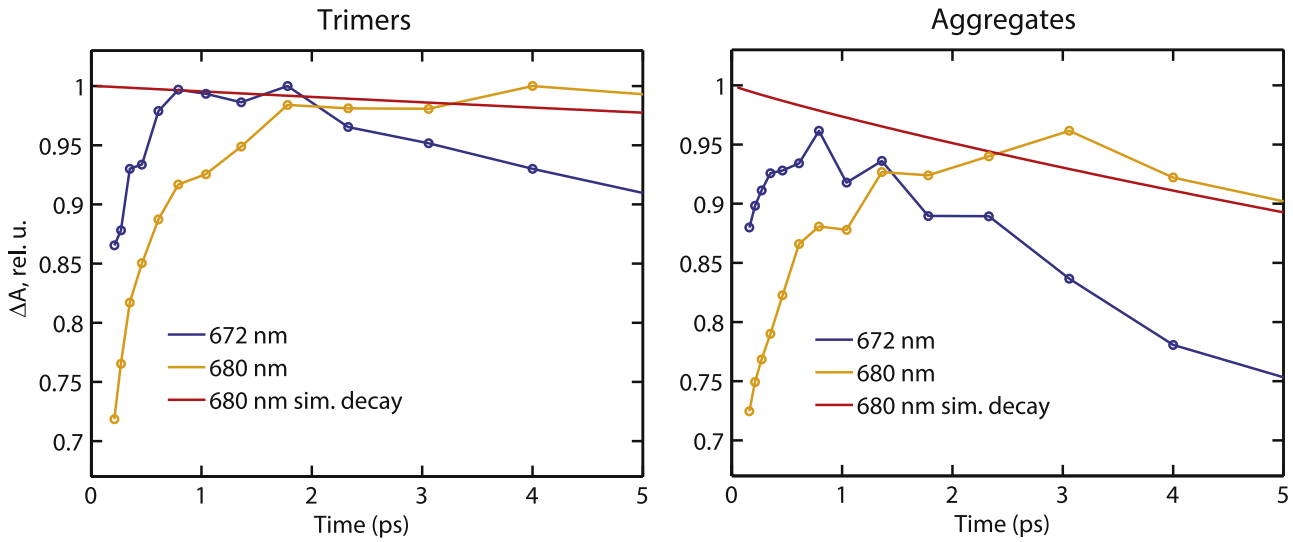

FIG. 7. Comparison of decay of Chl *a* signals at $\lambda_3 = 672$ and 680 nm in trimers and aggregates. The kinetic traces are integrated signals from the 2D spectra recorded using low power excitation (10 nJ). The red lines represent the simulated Chl *a* decay based on TCSPC measurement shown in Fig. S2.[57]

simulated curve represents excited-state decay in the absence of energy transfer; hence, it does not rise in the first 2 ps. The curve shows that together annihilation and quenching of the thermally equilibrated excited states can only recover about 10% of the ground state within 5 ps. Evidently, the measured kinetic curve at $\lambda_1 = 672$ nm decays more rapidly (25% decay in 5 ps). Therefore, it can be confirmed that the intermediate states around 672 nm decay via an intrinsic pathway, which cannot be accounted for by singlet–singlet annihilation.

C. On the identity of the intermediate states

Based on the results presented here, we can only speculate about the possible causes for the accelerated decay of the intermediate Chl *a* state. Mostly because of its short lifetime, it can be argued that the underlying process is not related to quenching by a specific molecular species, such as, e.g., a zeaxanthin or other carotenoid with low-lying energy level, but is exciton or exciton-charge-transfer state equilibration in which the donor is an intermediate-energy (~670–675 nm) Chl *a* exciton state. More likely, it is a result of acceleration of the Chl-Chl energy transfer upon aggregation, either due to a conformational change in the trimeric complex or, possibly, due to interactions between Chls in adjacent trimers.

Recent structure-based exciton calculations of LHCII by Müh and Renger[56] predicted red-shift of site energies (and consequently exciton energies) of specific Chl *a* molecules upon aggregation of solubilized trimers. A 3 nm red-shift of site energies was calculated for Chls *a*603 and *a*610 which absorb at 676 nm and 679 nm, respectively, in the aggregated state. A 1–2 nm red-shift in energy was calculated for Chls *a*611, *a*612, and *a*613 with site energy positions between 670 and 676 nm. These Chl *a* pigments are within the vicinity of the 2 lutein pigments which may have undergone reorientations upon protein aggregation thereby inducing environmental changes which affect the Chl site energies.[56] The reorientations and changes in energy levels may be the reason for altered energy transfer kinetics but are small enough so that 2D cross-peaks in trimers could be attributed to the same pigment groups. Aggregation also results in slight variations of the site energies of some Chl *b* molecules—Chls *b* 601 and 607 are shifted by 2-3 nm in aggregates. These shifts too are small enough so that we can assume the same excitation distribution induced by the pump pulses for both types of LHCII.

As to the pigment moieties responsible for the long-lived energy states, plausible candidates are Chls *a* located on the lumenal side of the complex, i.e., Chls 604, 613, and 614, which are relatively distant from the lowest-energy Chl clusters. Previously, the "bottleneck" state was assumed to be on Chl 604,[5,35] but calculations by Renger *et al.*[8] predict, on one hand, red-shifted Chl 604 and, on the other hand, slow energy transfer (tens of ps) from Chl 613/614. It remains a possibility, albeit unlikely, that in aggregates, fast energy transfer (~3 ps time scale) occurs from the peripherally positioned Chl 613/614 pair to Chls on the nearest neighbour complex.

D. Conclusion

In summary, in this work, we have uncovered a long-lived intermediate exciton state in LHCII trimers, which becomes strongly coupled to lower-lying states and respectively short-lived upon aggregation. While this change does not necessarily have a major influence on the overall excited-state dynamics, it does signify that the change in the environment of LHCII can affect not only the dynamics of the lowest-lying energy states but also the pathways and dynamics of energy transfer between higher intermediate states. Our case study also demonstrates that minor changes in the energy-transfer dynamics of a highly complex system can potentially be detected by room-temperature 2DES, which would be of great importance, for instance, in engineering photoactive pigment-protein complexes for performing specialized functions or improving their efficiency.

ACKNOWLEDGMENTS

This work is supported by a joint grant from the Singapore Agency for Science, Technology and Research, A*STAR, and

the Hungarian National Innovation Office (A*STAR SERC Grant No. 102-149-0153 and NIH-A*STAR TET_10-1-2011-027), a grant from the Singapore National Research Foundation (No. NRF-CRP5-2009-04, to H.S.T.), and a grant from the Hungarian Research Fund (No. OTKA-PD 104530 to P.L. and No. K112688 to G.G.).

[1]R. Blankenship, *Molecular Mechanisms of Photosynthesis*, 2nd ed. (Wiley-Blackwell, Oxford, UK, 2014).
[2]Z. F. Liu, H. C. Yan, K. B. Wang, T. Y. Kuang, J. P. Zhang, L. L. Gui, X. M. An, and W. R. Chang, Nature **428**, 287 (2004).
[3]A. A. Pascal, Z. Liu, K. Broess, B. van Oort, H. van Amerongen, C. Wang, P. Horton, B. Robert, W. Chang, and A. Ruban, Nature **436**, 134 (2005).
[4]J. Standfuss, A. C. T. van Scheltinga, M. Lamborghini, and W. Kühlbrandt, EMBO J. **24**, 919 (2005).
[5]V. I. Novoderezhkin, M. A. Palacios, H. van Amerongen, and R. van Grondelle, J. Phys. Chem. B **109**, 10493 (2005).
[6]R. van Grondelle and V. I. Novoderezhkin, Phys. Chem. Chem. Phys. **8**, 793 (2006).
[7]F. Müh, M. E.-A. Madjet, and T. Renger, J. Phys. Chem. B **114**, 13517 (2010).
[8]T. Renger, M. E. Madjet, A. Knorr, and F. Müh, J. Plant Physiol. **168**, 1497 (2011).
[9]J. Linnanto, J. Martiskainen, V. Lehtovuori, J. Ihalainen, R. Kananavicius, R. Barbato, and J. Korppi-Tommola, Photosynth. Res. **87**, 267 (2006).
[10]P. Horton, A. V. Ruban, and R. G. Walters, Annu. Rev. Plant Physiol. Plant Mol. Biol. **47**, 655 (1996).
[11]P. Müller, X.-P. Li, and K. K. Niyogi, Plant Physiol. **125**, 1558 (2001).
[12]P. Horton and A. Ruban, J. Exp. Bot. **56**, 365 (2005).
[13]P. Horton, A. V. Ruban, D. Rees, A. A. Pascal, G. Noctor, and A. J. Young, FEBS Lett. **292**, 1 (1991).
[14]C. W. Mullineaux, A. A. Pascal, P. Horton, and A. R. Holzwarth, Biochim. Biophys. Acta, Bioenerg. **1141**, 23 (1993).
[15]S. Vasil'ev, K.-D. Irrgang, T. Schrötter, A. Bergmann, H.-J. Eichler, and G. Renger, Biochemistry **36**, 7503 (1997).
[16]N. M. Magdaong, M. M. Enriquez, A. M. LaFountain, L. Rafka, and H. A. Frank, Photosynth. Res. **118**, 259 (2013).
[17]Y. Miloslavina, A. Wehner, P. H. Lambrev, E. Wientjes, M. Reus, G. Garab, R. Croce, and A. R. Holzwarth, FEBS Lett. **582**, 3625 (2008).
[18]A. R. Holzwarth, Y. Miloslavina, M. Nilkens, and P. Jahns, Chem. Phys. Lett. **483**, 262 (2009).
[19]A. V. Ruban, M. P. Johnson, and C. D. P. Duffy, Biochim. Biophys. Acta, Bioenerg. **1817**, 167 (2012).
[20]A. V. Ruban, R. Berera, C. Ilioaia, I. H. M. van Stokkum, J. T. M. Kennis, A. A. Pascal, H. van Amerongen, B. Robert, P. Horton, and R. van Grondelle, Nature **450**, 575 (2007).
[21]M. G. Müller, P. Lambrev, M. Reus, E. Wientjes, R. Croce, and A. R. Holzwarth, ChemPhysChem **11**, 1289 (2010).
[22]N. E. Holt, D. Zigmantas, L. Valkunas, X.-P. Li, K. K. Niyogi, and G. R. Fleming, Science **307**, 433 (2005).
[23]S. Bode, C. C. Quentmeier, P.-N. Liao, N. Hafi, T. Barros, L. Wilk, F. Bittner, and P. J. Walla, Proc. Natl. Acad. Sci. U. S. A. **106**, 12311 (2009).
[24]K. R. Naqvi, T. Jávorfi, T. B. Melø, and G. Garab, Spectrochim. Acta, Part A **55**, 193 (1999).
[25]M. Wahadoszamen, R. Berera, A. M. Ara, E. Romero, and R. van Grondelle, Phys. Chem. Chem. Phys. **14**, 759 (2012).
[26]A. Kell, X. Feng, C. Lin, Y. Yang, J. Li, M. Reus, A. R. Holzwarth, and R. Jankowiak, J. Phys. Chem. B **118**, 6086 (2014).
[27]H. M. Visser, F. J. Kleima, I. H. M. van Stokkum, R. van Grondelle, and H. van Amerongen, Chem. Phys. **210**, 297 (1996).
[28]J. P. Connelly, M. G. Müller, M. Hucke, G. Gatzen, C. W. Mullineaux, A. V. Ruban, P. Horton, and A. R. Holzwarth, J. Phys. Chem. B **101**, 1902 (1997).
[29]V. I. Novoderezhkin and R. van Grondelle, Phys. Chem. Chem. Phys. **12**, 7352 (2010).
[30]F. J. Kleima, C. C. Gradinaru, F. Calkoen, I. H. M. van Stokkum, R. van Grondelle, and H. van Amerongen, Biochemistry **36**, 15262 (1997).
[31]D. M. Jonas, Annu. Rev. Phys. Chem. **54**, 425 (2003).
[32]M. Cho, Chem. Rev. **108**, 1331 (2008).
[33]J. D. Hybl, A. W. Albrecht, S. M. G. Faeder, and D. M. Jonas, Chem. Phys. Lett. **297**, 307 (1998).
[34]T. Brixner, T. Mančal, I. V. Stiopkin, and G. R. Fleming, J. Chem. Phys. **121**, 4221 (2004).
[35]G. S. Schlau-Cohen, T. R. Calhoun, N. S. Ginsberg, E. L. Read, M. Ballottari, R. Bassi, R. van Grondelle, and G. R. Fleming, J. Phys. Chem. B **113**, 15352 (2009).
[36]G. S. Schlau-Cohen, A. Ishizaki, and G. R. Fleming, Chem. Phys. **386**, 1 (2011).
[37]K. L. Wells, P. H. Lambrev, Z. Zhang, G. Garab, and H.-S. Tan, Phys. Chem. Chem. Phys. **16**, 11640 (2014).
[38]S. Caffarri, R. Croce, J. Breton, and R. Bassi, J. Biol. Chem. **276**, 35924 (2001).
[39]S. X. Yan and H.-S. Tan, Chem. Phys. **360**, 110 (2009).
[40]Z. Zhang, K. L. Wells, E. W. J. Hyland, and H.-S. Tan, Chem. Phys. Lett. **550**, 156 (2012).
[41]H.-S. Tan, J. Chem. Phys. **129**, 124501 (2008).
[42]A. Monmayrant, A. Arbouet, B. Girard, B. Chatel, A. Barman, B. J. Whitaker, and D. Kaplan, Appl. Phys. B **81**, 177 (2005).
[43]F. Verluise, V. Laude, Z. Cheng, C. Spielmann, and P. Tournois, Opt. Lett. **25**, 575 (2000).
[44]G. S. Schlau-Cohen, A. Ishizaki, T. R. Calhoun, N. S. Ginsberg, M. Ballottari, R. Bassi, and G. R. Fleming, Nat. Chem. **4**, 389 (2012).
[45]A. Ishizaki and G. R. Fleming, J. Chem. Phys. **130**, 234111 (2009).
[46]T. Bittner, K. D. Irrgang, G. Renger, and M. R. Wasielewski, J. Phys. Chem. **98**, 11821 (1994).
[47]V. Barzda, V. Gulbinas, R. Kananavicius, V. Cervinskas, H. van Amerongen, R. van Grondelle, and L. Valkunas, Biophys. J. **80**, 2409 (2001).
[48]P. H. Lambrev, F.-J. Schmitt, S. Kussin, M. Schoengen, Z. Várkonyi, H. J. Eichler, G. Garab, and G. Renger, Biochim. Biophys. Acta, Bioenerg. **1807**, 1022 (2011).
[49]A. V. Ruban, A. A. Pascal, B. Robert, and P. Horton, J. Biol. Chem. **276**, 24862 (2001).
[50]P. Lambrev, Z. Várkonyi, S. Krumova, L. Kovács, Y. Miloslavina, A. R. Holzwarth, and G. Garab, Biochim. Biophys. Acta, Bioenerg. **1767**, 847 (2007).
[51]C. Ilioaia, M. P. Johnson, P. Horton, and A. V. Ruban, J. Biol. Chem. **283**, 29505 (2008).
[52]P. Akhtar, M. Dorogi, K. Pawlak, L. Kovács, A. Bóta, T. Kiss, G. Garab, and P. H. Lambrev, J. Biol. Chem. **290**, 4877 (2015).
[53]R. Croce, M. G. Müller, R. Bassi, and A. R. Holzwarth, Biophys. J. **84**, 2508 (2003).
[54]L. Valkunas, I. H. M. van Stokkum, R. Berera, and R. van Grondelle, Chem. Phys. **357**, 17 (2009).
[55]D. Rutkauskas, J. Chmeliov, M. Johnson, A. Ruban, and L. Valkunas, Chem. Phys. **404**, 123 (2012).
[56]F. Müh and T. Renger, Biochim. Biophys. Acta, Bioenerg. **1817**, 1446 (2012).
[57]See supplementary material at http://dx.doi.org/10.1063/1.4919239 for statistical errors of the global lifetime analysis, 2D DAS of trimers and aggregates at 10 nJ, description of kinetic modelling of the rates of singlet–singlet annihilation, and fluorescence decay kinetics.